Preprints (www.preprints.org) | NOT PEER-REVIEWED | Posted: 8 November 2021 doi:10.20944/preprints202111.0155.v1

Article

Amphiphilic carboxymethyl dextran nanomicelles for antibacterial coating on titanium

Hongbo Wei [1, †, *], Minghao Zhou [1, †], Luxuan Zhang [2], Jingwei Yu [2], Weiliang Ye [3,*]

[1] State Key Laboratory of Military stomatology, National clinical research center for Oral Diseases & Shaanxi engineering research center for Dental Materials and advanced Manufacture, Department of Oral Implants, School of stomatology, The Fourth Military Medical University, Xi'an, People's republic of China; caironchow@gmail.com

[2] Department of Basic Medical, School of Basic Medical, Fourth Military Medical University, Xi'an, People's Republic of China; zlx1323917280@163.com

[3] Department of Pharmaceutics, School of Pharmacy, Fourth Military Medical University, Xi'an, People's republic of China;

* Correspondence: yaojixue@fmmu.edu.cn (W.Y.) ; weihongbo101@126.com (H.B.)

† These authors contributed equally to this work.

Abstract: Peri-implantitis occurs at a significant rate, which is the leading cause of implant failure. The main reason for this unwanted complication is bacterial invasion and biofilm formation. To reduce the incidence of peri-implantitis, we constructed a carboxymethyl dextran (CMD) based nanomicelles antibacterial coating on microarc-oxidized titanium (MAO-Ti) surface. After cross-linking, the drug-loaded nanomicelles were spherical with a particle size of 130nm and uniformly dispersed. Zeta potential was negative, and the absolute value was greater than 10 mV, effectively avoiding micelles aggregation. It was observed by dynamic light scattering (DLS) that the stability of nanomicelles was significantly improved after cross-linking. The hemolysis rate of micelles was less than 5%, and the overall survival rate of human umbilical vein endothelial cells was more than 90%. After being coated on MAO-Ti surface, the cumulative drug release rate of drug-loaded nanomicelles reached 86.6% after 360 hours. Fluorescence staining of immobilized bacteria showed more dead bacteria on the coating surface, and the number of live bacteria was significantly reduced. It was concluded that dextran-based nanomicelles, which showed long-term drug release properties and excellent biocompatibility, are potential drug carriers for fabricating antibacterial coating on titanium surfaces.

Keywords: nanomaterials; microarc oxidation; dextran; minocycline; titanium; antibacterial coating

1. Introduction

Epidemiologically, the prevalence of peri-implantitis ranged from 22% to 56% [1]. Other similar meta-analyses during the same period reported that the incidence of implants was 12.9%. ~28% [2,3]. This discrepancy was mainly derived from varying clinical diagnostic criteria. Clinically, peri-implantitis is one of the major causes of dental implant failure, resulting in nearly 4% implant loss [4].

The invasion of microorganisms and bacterial biofilm formation is the fundamental reasons for the inflammation of soft tissue around the implant [5-8]. The implant's surface is usually mechanically polished in clinic, which is poorly integrated with the surrounding soft tissues. Furthermore, the binding site with the soft tissue is directly exposed to the bacterial environment. Thus, it is highly susceptible to being invaded by bacteria in the process of implantation and healing, which causes inflammation and ultimately results in the failure of the implant [6,9].

The preparation of antibacterial coating by implant surface modification is an effective strategy to reduce the incidence of implant-related infection [10,11]. Compared with systemic administration, the preparation of antibiotic coatings on the surface of implants

© 2021 by the author(s). Distributed under a Creative Commons CC BY license.

Preprints (www.preprints.org) | NOT PEER-REVIEWED | Posted: 8 November 2021 doi:10.20944/preprints202111.0155.v1

can achieve a high local drug concentration around the implant, avoid systemic toxicity and prevent bacterial drug resistance [12,13]. Some scholars have started to explore this field. Çalışkan et al. used a simple adsorption method to load gentamicin onto the surface of TiO2 nanotubes, and it was found that the coated titanium had a significant antibacterial effect on *S. aureus* in vitro [14]. Our research group had also made explorations in the early stage [15]. Nevertheless, these studies still showed a small drug loading and short sustained release time.

In recent years, nanomicelles, due to their small particle size, excellent stability, high drug loading, sustained release, have been applied in various biological and medical fields, such as Cancer-targeted therapy [16-19] , and ophthalmologic disease [20]. Nanomicelles are nano-sized colloidal carriers characterized by core-shell structures consisting of the exterior hydrophilic polar head and interior hydrophobic tail. When critical micelle concentration (CMC) is reached, amphiphilic molecules can bury the hydrophobic drugs within their hydrophobic core while self-assembling [21]. Dextran, as a biopolymer, has many advantages over synthetic polymers in the construction of nanomicelles for drug delivery, such as excellent solubility in water, biocompatibility, and non-toxicity [22,23]. However, to the best of our knowledge, amphiphilic dextran-based nanomicelles have not been exploited to develop antimicrobial coatings on titanium.

Minocycline (MC) is a kind of antibacterial agent widely used in periodontitis and peri-implantitis, which has an apparent antibacterial effect on the pathogenic flora of peri-implantitis [24,25]. It can bind to the A position of bacterial ribosomal 30S subunit and inhibit protein synthesis by preventing the extension of peptide chains, thus producing the antimicrobial effect.

In this study, to develop amphiphilic nanomicelles, CMD was chemically modified with octadecylamine (ODA) through the formation of stable amide bonds. MC, used as the model antibiotic, was encapsulated into the hydrophobic core of nanomicelles by the dialysis method. Finally, we constructed shell crosslinked MC-loaded nanomicelles (MC@(ODA-CMD)$_{CL}$) on the MAO-Ti surface. The drug-loaded nanomicelles' characteristics were evaluated, and the drug-release performance, the antibacterial properties, and the possible influence on human cells were analyzed.

2. Results

2.1. Characterization of ODA-CMD

ODA-CMD becomes a white loose solid after freeze-drying, and it was identified by Proton nuclear magnetic resonance (^{1}HNMR). As shown in Figure 1A, the chemical shift of protons on the glucoside ring of glucan appears at 3.15-3.85 ppm. 4.25-5.12 ppm is the chemical shift of the hydroxyl protons on the glucan and the protons on the heterotopic carbon. 0.85 and 1.24-1.5 PPM can be referred to as the end methyl on the octadecylamine and intermediate methylene proton peak, respectively. The chemical shift 4.12ppm is the upper methylene proton peak after carboxymethylation of dextran. 3.09ppm is assigned to the proton peak of methylene closest to the amide bond.

The polymer materials were identified by Fourier Transform infrared spectroscopy (FTIR). As shown in Figure 1B, the characteristic peak at 1689 cm-1 comes from the stretching vibration of the amide bond C=O, the characteristic peak at 1530 cm-1 comes from the stretching vibration of the amide bond N-H, the characteristic peak at 1290 cm-1 comes from the stretching vibration of the amide bond C-N, and the absorption peak of 1655 cm-1 is produced by the hydrogen bond H-O-H of the dextran. The above results confirm that the synthetic polymer ODA-CMD is the target material.

Preprints (www.preprints.org) | NOT PEER-REVIEWED | Posted: 8 November 2021 doi:10.20944/preprints202111.0155.v1

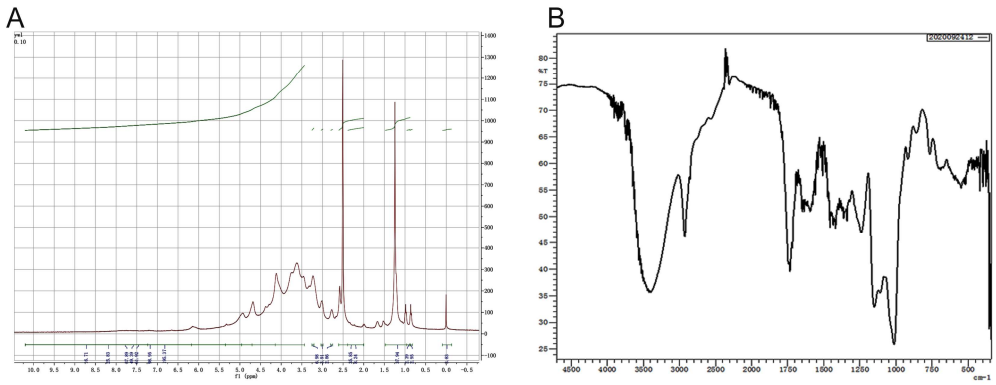

Figure 1. (A) ^{1}H NMR spectra of ODA-CMD **(B)** Infrared spectra of ODA-CMD

2.2. Characterization of drug-loaded nanomicelles

As shown in Table 1, the particle size of MC@(ODA-CMD)$_{CL}$ is 130nm, and that of MC@ODA-CMD is 118nm. The PDI value indicates that the micelle particle size is evenly distributed. The Zeta potentials of the two types of micelles are negative, and the absolute value is greater than 10 mV, which can effectively avoid the aggregation of micelles and maintain the stability of the micelles. The drug loading and encapsulation rate of MC@(ODA-CMD)$_{CL}$ were slightly higher than those of MC@ODA-CMD. In addition, the CMC value of MC@(ODA-CMD)$_{CL}$ is also significantly lower than that of MC@ODA-CMD, and the lower CMC value indicates that the crosslinked micelle MC@(ODA-CMD)$_{CL}$ possesses better stability. The transmission electron microscopy (TEM) results of MC@ODA-CMD and MC@(ODA-CMD)$_{CL}$ are shown in Figure 2 (A and B). It can be seen that MC@(ODA-CMD)$_{CL}$ and MC@ODA-CMD are spherical and well dispersed. The particle size distributions of MC@(ODA-CMD)$_{CL}$ and MC@ODA-CMD were determined by DLS. The results are shown in Figure 2 (C and D). The particle size of micelles measured by TEM is smaller than that measured by DLS. This is because of the shrinkage of micelles under the dry condition when TEM is observed. The scanning results of the ultraviolet spectrophotometer (Figure 2E) show that MC@(ODA-CMD)$_{CL}$ and MC@ODA-CMD have the characteristic absorption peak of MC, while the blank material does not have any ultraviolet absorption. The results further indicate that the drug-loaded micelle successfully encapsulated MC and did not affect its structure.

Table 1. Characteristics of drug-loaded micelles. n=3，$\bar{x}$ ± s

Micelles	Size（nm）	PDI	Zeta（mV）	DL（%）	EE（%）	CMC（mg/L）
MC@ODA-CMD	118±10	0.21±0.03	−18.6±1.9	15.67±0.2	43.84±5.3	4.9
MC@(ODA-CMD)$_{CL}$	130±16	0.19±0.08	−14.3±2.3	17.31±0.8	50.18±3.8	3.1*

Abbreviations: PDI, polymer dispersity index; DL, drug-loading; EE, encapsulation efficiency; CMC, critical micelle concentration.

Preprints (www.preprints.org) | NOT PEER-REVIEWED | Posted: 8 November 2021 doi:10.20944/preprints202111.0155.v1

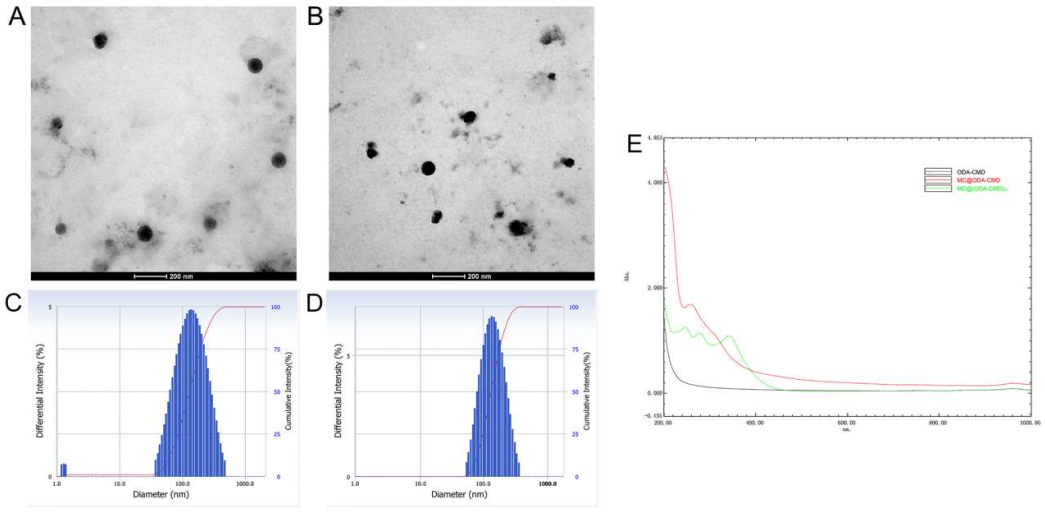

Figure 2. TEM images of (A) MC@ODA-CMD and (B) MC@(ODA-CMD)$_{CL}$; DLS of (C) MC@ODA-CMD and (D) MC@(ODA-CMD)$_{CL}$; (E) Ultraviolet spectrophotometer scanning results of MC@ODA-CMD and MC@(ODA-CMD)$_{CL}$.

2.3. Stability of drug-loaded nanomicelles

The changes of particle size and PDI of MC@(ODA-CMD)$_{CL}$ and MC@ODA-CMD incubated in pH 7.4 PBS buffer for 30 days were investigated by DLS (Figure 3C and D). The particle size of MC@ODA-CMD suddenly increased after 10 days, and PDI increased as well (Figure 3A), while the particle size and PDI of MC@(ODA-CMD)$_{CL}$ did not change significantly within 30 days (Figure 3B). The morphological changes of MC@(ODA-CMD)$_{CL}$ and MC@ODA-CMD incubated in PBS buffer with pH 7.4 for 30 days were observed by TEM. It can be seen from Figure 3F that the size of MC@(ODA-CMD)$_{CL}$ slightly increased after incubated in pH 7.4 buffer for 30 days, and the micellar morphology can still be observed. After incubated in a buffer for 30 days, however, MC@ODA-CMD was dissolved entirely, and the micellar morphology can not be observed (Figure 3E). The above results indicated that the stability of micelles was significantly improved after crosslinking, which laid a foundation for its long-term drug release.

Preprints (www.preprints.org) | NOT PEER-REVIEWED | Posted: 8 November 2021 doi:10.20944/preprints202111.0155.v1

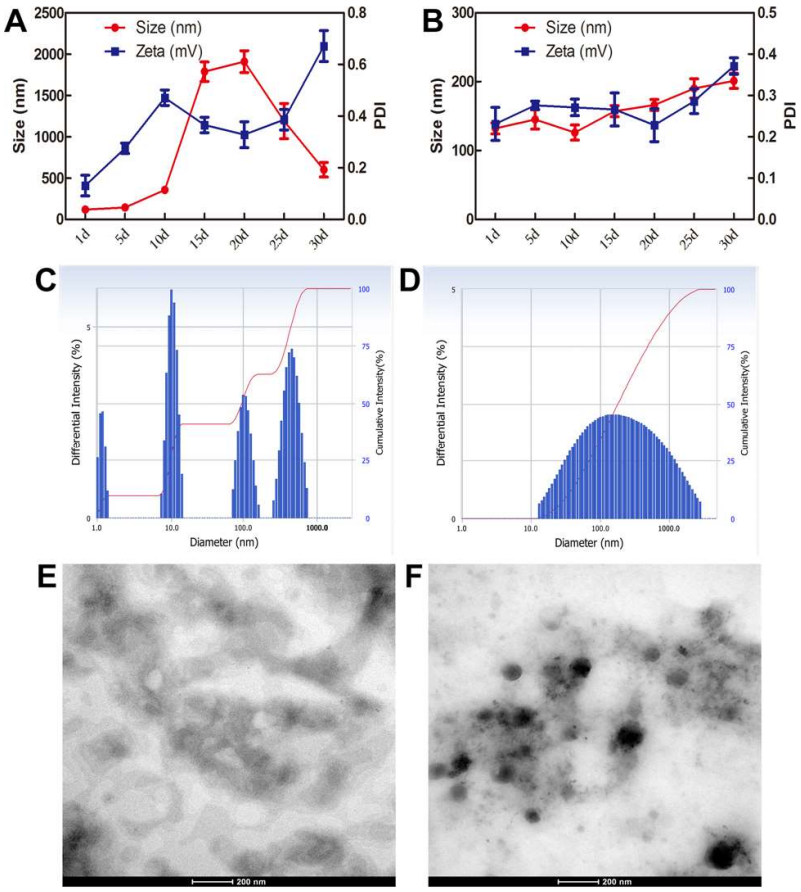

Figure 3. (A) The changes of particle size of MC@ODA-CMD and **(B)** MC@(ODA-CMD)$_{CL}$ incubated in PBS buffer for 30 days. DLS results of particle size of **(C)** MC@ODA-CMD and **(D)** MC@(ODA-CMD)$_{CL}$ incubated in PBS buffer for 30 days. TEM images of **(E)** MC@ODA-CMD and **(F)** MC@(ODA-CMD)$_{CL}$ incubated in PBS buffer for 30 days.

2.4. Biocompatibility of micellar materials

The hemolysis experiment can be used to assess the biocompatibility of biomaterials, and it is reported that the hemolysis rate of less than 5% is the essential requirement for the application of biomaterials in medicine[26]. The hemolysis photograph of two kinds of blank micelles at different concentrations incubated with rabbit whole blood for 60 mins is shown in Figure 4. The statistical result is shown in Figure 5. In sharp contrast to the distilled water-treated group, no apparent rupture was found in ODA-CMD and (ODA-CMD)$_{CL}$ treated groups. The hemolysis rate is concentration-dependent, but two kinds of blank micelles showed less than 5% hemolysis rate even at high concentration, and there was no significant difference between ODA-CMD and (ODA-CMD)$_{CL}$ groups. These results indicated that two kinds of blank micelles materials showed no damage to RBCs when the concentration was less than 1.0mg/mL. The toxicity of ODA-CMD and (ODA-CMD)$_{CL}$ against HUVECs is shown in Figure 6. The viability of HUVECs treated with different concentrations of ODA-CMD and (ODA-CMD)$_{CL}$ has no significant change, and the overall viability rate of HUVECs was above 90%. These results showed that two kinds of micellar materials had no toxic effect on HUVECs.

Preprints (www.preprints.org) | NOT PEER-REVIEWED | Posted: 8 November 2021 doi:10.20944/preprints202111.0155.v1

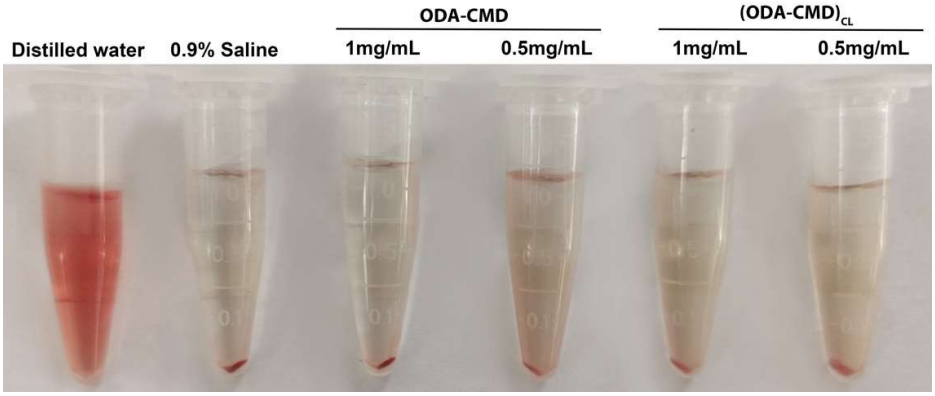

Figure 4. (A) The changes of particle size of MC@ODA-CMD and **(B)** MC@(ODA-CMD)$_{CL}$ incubated in PBS buffer for 30 days. DLS results of particle size of **(C)** MC@ODA-CMD and **(D)** MC@(ODA-CMD)$_{CL}$ incubated in PBS buffer for 30 days. TEM images of **(E)** MC@ODA-CMD and **(F)** MC@(ODA-CMD)$_{CL}$ incubated in PBS buffer for 30 days.

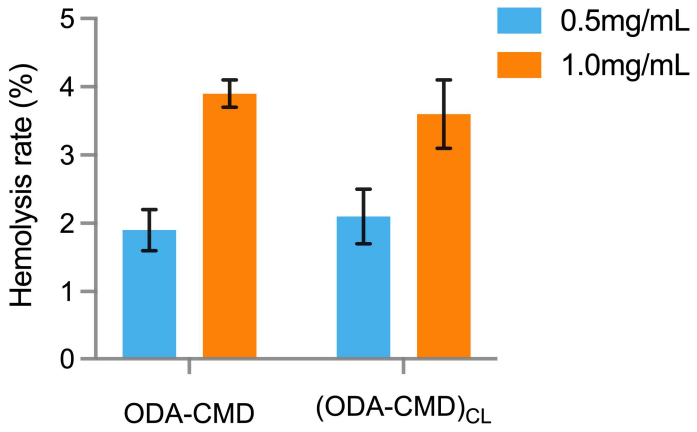

Figure 5. Hemolysis rate of rabbit RBCs with two kinds of blank nanomicelles at different concentrations

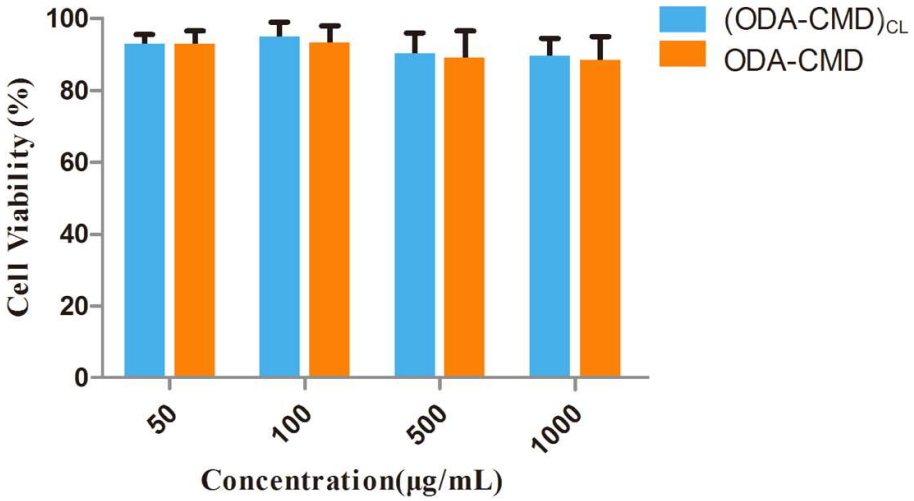

Figure 6. Cell viability in HUVECs after treatment with two kinds of blank micelles for 24h.

Preprints (www.preprints.org) | NOT PEER-REVIEWED | Posted: 8 November 2021 doi:10.20944/preprints202111.0155.v1

2.5. Release property of drug-loaded micellar coating on titanium surface

The results of accumulative drug release of MC from different specimens at various period is shown in Figure 7. For free MC, the drug release was mainly through the free diffusion of concentration difference, and the cumulative drug release reached 94% after 72 hours. When free MC was coated on titanium sheet, the drug release property was similar to that of free MC, and the cumulative drug release reached 90% after 96h. For MC@(ODA-CMD)$_{CL}$ and MC@ODA-CMD, the drug release pattern could be divided into two phases. The release rate was relatively fast in the first phase, known as the initial burst release. This was probably due to the release of the drugs without being encapsulated into the core of nanomicelles, and these parts of drugs were absorbed on the surface of nanomicelles through a weak binding force even though nanomicelles were rinsed by distilled water. In the second phase, the drugs maintained a long-term sustained release. The cumulative drug release rate of MC@(ODA-CMD)$_{CL}$ was 88% after 312h, while that of MC@ODA-CMD was found to be 89% after 168h. This result showed that the sustained release performance of crosslinked nanomicelles MC@(ODA-CMD)$_{CL}$ was better than that of uncrosslinked nanomicelles MC@(ODA-CMD). In addition, after MC@(ODA-CMD)$_{CL}$ and MC@ODA-CMD were coated on MAO-Ti, their respective release times were slightly prolonged, but the highest cumulative release rates of both were almost maintained at the same level, in which the former's release rate reached 86.6% after 360h and the latter's release rate was 87.5% after 216h.

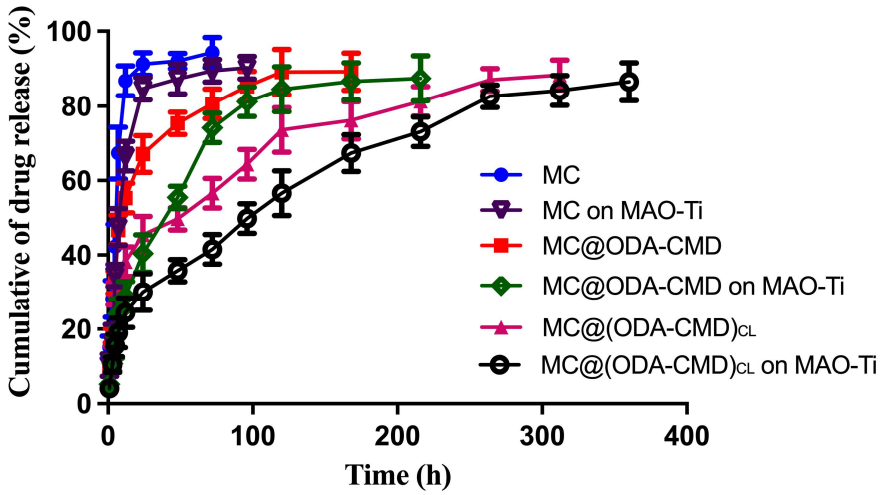

Figure 7. The accumulative drug release of MC from different specimens at various periods of time.

2.6. Characterization of titanium specimens

Representative scanning electron microscope (SEM) photographs of the titanium specimens are shown in Figure 8. The smooth titanium (S-Ti) surface was relatively smooth after being ground by silicon carbide paper (Figure 8A). The titanium surface after MAO treatment possessed a porous morphology with pores of 1-5 μm, which can provide many footholds for loading of drug-loaded nanomicelles (Figure 8B). It can be seen from Figure 8C that drug-loaded nanomicelles were loaded within the pores on the MAO-Ti surface after oscillation and cross-linking.

Preprints (www.preprints.org) | NOT PEER-REVIEWED | Posted: 8 November 2021 doi:10.20944/preprints202111.0155.v1

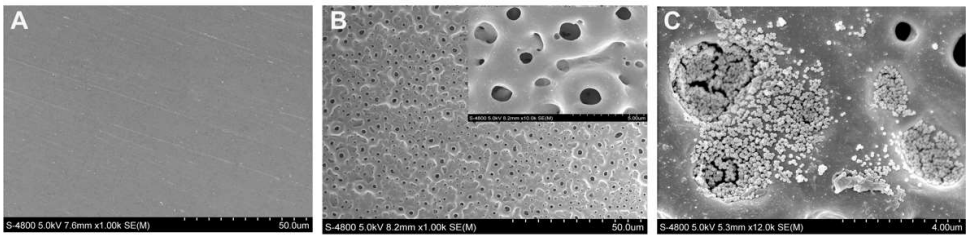

Figure 8. SEM photographs of **(A)** smooth titanium surface, **(B)** microarc-oxidized titanium surface under low magnification, and (inset) under high magnification **(C)** microarc-oxidized titanium surface with antibacterial coating.

2.7. Antibacterial effects

To quantitatively analyze the antibacterial effect of the specimens including planktonic and immobilized bacteria, bacteria colony counting was carried out. From the photographs of bacteria colonies on the Mueller-Hinton agar (MHA) plates, we found that the number of bacterial colonies on MC@(ODA-CMD)$_{CL}$ -MAO-Ti (Figure 9C) was the least compared to that of S-Ti (Figure 9A) and MAO-Ti (Figure 9B). The quantification results demonstrated that the antibacterial rate (AR) of MC@(ODA-CMD)$_{CL}$-Ti specimen was 67.3%, while the MAO-Ti specimen possessed an AR value of -443.6%.

To detect the viability of bacteria after contacting with MC@(ODA-CMD)$_{CL}$-Ti, we carried out bacterial fluorescence staining, and the results were consistent with quantitative results. We found that most of the bacteria adhered to S-Ti (Figure 10A) and MAO-Ti (Figure 11B) were stained fluorescent green after 24 hours of incubation, indicating that they were alive and had intact membranes. In sharp contrast, almost all bacteria attached to MC@(ODA-CMD)$_{CL}$-Ti (Figure 10C) were fluorescent red, suggesting that they were dead with damaged membranes.

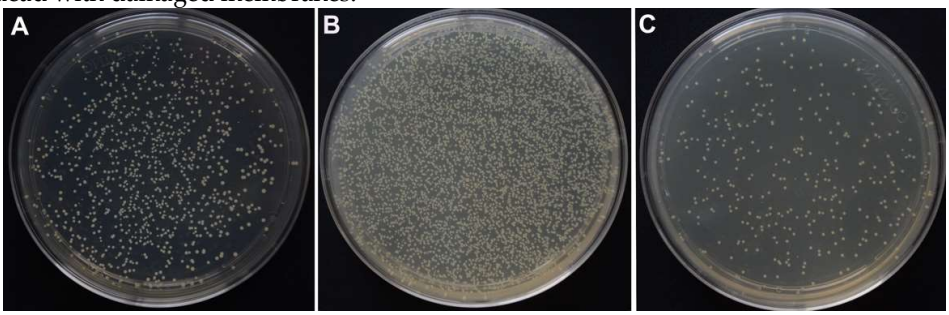

Figure 9. Bacteria colonies cultivated on MHA plates from **(A)** S-Ti, **(B)** MAO-Ti, and **(C)** MC@(ODA-CMD)$_{CL}$-MAO-Ti groups.

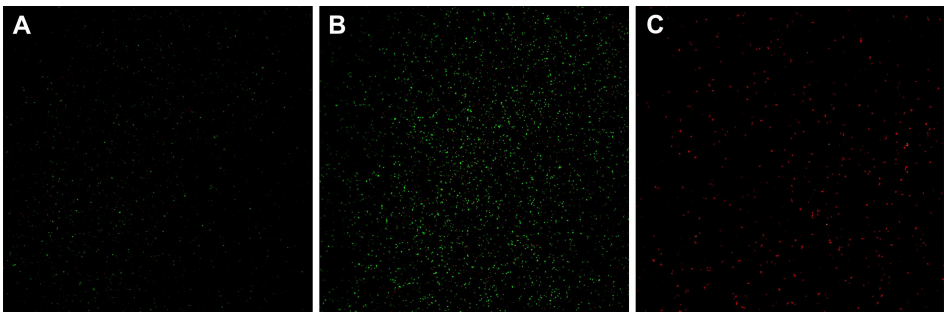

Figure 10. Fluorescence microscopy photographs showing *S.aureus* on various specimens after SYTO ® 9/propidium iodide staining. **(A)** S-Ti; **(B)** MAO-Ti; **(C)** MC@(ODA-CMD)$_{CL}$-MAO-Ti,

Preprints (www.preprints.org) | NOT PEER-REVIEWED | Posted: 8 November 2021 doi:10.20944/preprints202111.0155.v1

3. Discussion

Compared with natural teeth, certain histological and morphological defects exist in the soft tissue around the dental implant, such as weak integration between the implant surface and junctional epithelium, lack of periodontal ligament, and less blood supply [27,28]. In addition, the oral cavity is a complex environment containing multiple types of microorganism, which is prone to bacterial adhesion and invasion [29]. Studies have shown that initial bacterial adhesion and biofilm formation are the main causes of peri-implant-associated infection [13]. Thus, many scholars have adopted various strategies to build antibacterial coatings on the surface of titanium to prevent bacterial infection. However, shortfalls still exist among these researches, such as insufficient drug release time and cytotoxicity [30-32].

Polymer nanomicelles are characterized by controllable function, simple synthetic process, high drug loading capacity, long sustained release time, excellent biocompatibility and stability [33], and thus substantial progress has been made in tumor-targeted treating fields [16,17]. In recent years, dextran and its derivatives based nanomicelles have been developed for drug delivery systems in medical applications [34]. The existence of α-1, 6 glycosidic bond in dextran provides an increase in chain mobility, which contribute to the high solubility of dextran in many solvents [22,35]. The nanomicelles prepared from dextran with high solubility can promote the dissolution of drugs and improve the drug bioavailability [22]. In addition, compared with other polysaccharides, dextran is not easily decomposed by salivary amylase and can only be broken down by dextranase in the liver, intestine, and kidney [36]. As a drug carrier nanomicelle for antibacterial coating on implant surface, good colloidal resistance against oral salivary amylase degradation is of great significance to maintain the integrity of drug delivery systems, prolong the drug release time and improve the drug bioavailability. To the best of our knowledge, dextran-based antibacterial coating on MAO-Ti surface has not been reported yet.

Considering that all processes of biofilm formation, from bacterial adhesion to biofilm maturation, are incredibly efficient, and they are usually completed within 12 to 18 hours [13,37,38]. Therefore, the antibacterial effect should play a role at the exact time of implantation or at least within a few hours or days. Besides, maintaining the minimum inhibitory concentration during the high-risk postoperative period is of significance for preventing implant-related infection [39]. Thus, high requirements are placed on the drug release time of antibacterial coating on titanium. Several studies have attempted to use various methods for sustained release. MC on graphene oxide modified titanium surface exhibited a slow-release behavior within 168 hours and showed excellent antibacterial effect [40]. Dextran-based amphiphilic polymers were used for sustained release of rapamycin within 7 days [41]. Our results showed that MC@(ODA-CMD)$_{CL}$ provided rapid initial release within the first 20 hours, followed by a long-term sustained release with 88% cumulative release rate after 312 hours. After being coated on MAO-Ti surface, the sustained release time reached 360 hours with 86.6% cumulative release rate. This biphasic profile can play a critical anti-infective role in the early stage of implantation and maintain the drug concentration at the treatment level during the sustained release phase.

MC is widely used in periodontitis and peri-implantitis and has an apparent antibacterial effect on the pathogenic bacteria of implant-associated infection. The primary mechanism of minocycline is to inhibit the protein synthesis of the bacterial ribosome. It can reversibly bind to the helical region (H34) of the 30S ribosome, preventing amino acid residues from being incorporated into the extended peptide chain, resulting in loss of peptide formation and bacterial growth [42]. According to a randomized clinical trial, MC microspheres could improve the probing depths and bleeding scores [43]. The antibacterial activity test showed that MC-loaded graphene oxide films on implant surface had a good therapeutic effect for peri-implantitis [44]. Thus, we chose MC as the model antibiotic in this study. In our research, minocycline loaded nanomicelles were successfully

Preprints (www.preprints.org) | NOT PEER-REVIEWED | Posted: 8 November 2021 doi:10.20944/preprints202111.0155.v1

prepared and stably loaded on the MAO titanium surface. TEM results show that MC@(ODA-CMD)$_{CL}$ is spherical with a particle size of about 130nm with good dispersion. The results of antibacterial rate and fluorescence staining demonstrate that MC-loaded nanomicells coating possesses good antibacterial ability against *S.aurues. S.aureus* is the most commonly found bacteria in the implant-related infection, which can adhere to the implant surface at the early stage and promote the accumulation of other bacteria resulting in the biofilm formation[13,37]. Thus, we expect the coating can exert promising effects in preventing bacterial invasion around implant.

At the same time, any coating technology should be proven safe over the short and long term since it is the fundamental requirement for further clinical application. Indeed, subcutaneous implantation studies and tissue response tests have demonstrated the biocompatibility of dextran-based delivery system, indicating that dextran shows no immunological reactions or toxicity to human cells [45,46]. These results were in accordance with ours. No cytotoxicity of dextran nanomicelles against human cells was observed in our investigation.

In summary, we provide a new strategy of nanomicelle antibacterial coating for implants. The results of this study show that drug-loaded nanomicelles based on amphiphilic CMD can stably carry sufficient antibiotics and show long-time sustained release in vitro with good biocompatibility. In other words, amphiphilic CMD is a potential drug carrier for preparing antibiotic coating on titanium surfaces. Our research has certain limitations. As the implant infection-related biofilm is composed of multiple bacteria, the antibacterial effects of other bacteria and experiments in vivo as well as the bonding strength of the coatings still need to be further examined, which will be considered in our future study.

4. Materials and Methods

4.1. Synthesis and characterization of Polymer Materials

4.1.1. Synthesis and characterization of ODA-CMD

The synthesis route of ODA-CMD is shown in Figure 11. 0.6g CMD (Carboxyl equivalent to 1mmol) (J&K Scientific Ltd, Beijing, China) and a small amount of lithium chloride (LICI) (Sigma-Aldrich, St Louis, USA) were dissolved in a certain amount of dimethylformamide (DMF). The solution was heated to 80℃ and stirred until completely dissolved. After cooling down to room temperature, 1-ethyl-3-(3-dimethylaminopropyl) carbodiimide hydrochloride/ N-hydroxysuccinimide (EDC/NHS) (J&K Scientific Ltd, Beijing, China) was added with stirring for activation for 1 hour. 0.5g (0.2mmol) ODA was dissolved in DMF. This solution was slowly dropwise added into the CMD (J&K Scientific Ltd, Beijing, China) solution and stirred at room temperature for 24 hours. After the reaction was finished, the white precipitate was obtained after repeatedly washing with a large amount of ice ethanol to remove unreacted oleylamine. Proton nuclear magnetic resonance (1H NMR) and FTIR spectra were recorded with Varian Mercury-Plus (300 MHz, USA) spectrometer and FTIR-8400S spectrometer (Shimadzu, Kyoto, Japan).

Preprints (www.preprints.org) | NOT PEER-REVIEWED | Posted: 8 November 2021 doi:10.20944/preprints202111.0155.v1

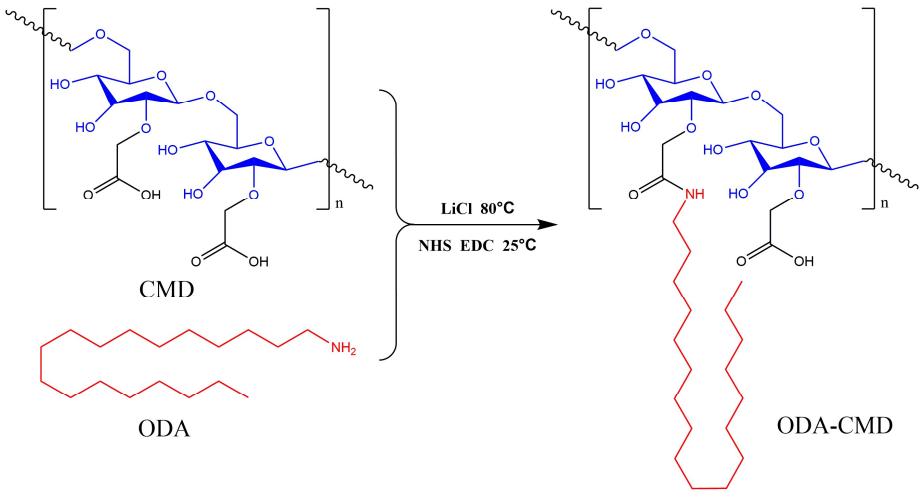

Figure 11. The synthesis route of ODA-CMD.

4.1.2. Synthesis and characterization of ODA-CMD

4mg minocycline hydrochloride (MC•HCl) (J&K Scientific Ltd, Beijing, China) was added to 4ml dimethyl sulfoxide (DMSO), then 4μL triethylamine (TEA) was added to the resulting solution after complete dissolution and was heated in an oil-bath at 60ºC with stirring protected from light exposure. 10mg polymer materials ODA-CMD were added into the reaction solution; after the mixture was stirred for 2h, a small amount of ethylenediamine for 16ml was slowly dropwise added and then stirred for another 12h. The mixture was packed into a dialysis bag (interception molecular weight:2000 Da) to dialyze in water for 48h, and the water was exchanged every 6h. The shell crosslinked drug-loaded micelle MC@(ODA-CMD) CL was obtained by freeze-drying after dialysis. In addition, uncross-linked drug-loaded micelle MC@ODA-CMD was prepared from distilled water without ethylenediamine as control.

4.1.3. Preparation of drug-loaded micelles

4mg minocycline hydrochloride (MC•HCl) (J&K Scientific Ltd, Beijing, China) was added to 4ml dimethyl sulfoxide (DMSO), then 4μL triethylamine (TEA) was added to the resulting solution after complete dissolution and was heated in an oil-bath at 60ºC with stirring protected from light exposure. 10mg polymer materials ODA-CMD were added into the reaction solution; after the mixture was stirred for 2h, a small amount of ethylenediamine for 16ml was slowly dropwise added and then stirred for another 12h. The mixture was packed into a dialysis bag (interception molecular weight:2000 Da) to dialyze in water for 48h, and the water was exchanged every 6h. The shell crosslinked drug-loaded micelle MC@(ODA-CMD) CL was obtained by freeze-drying after dialysis. In addition, uncross-linked drug-loaded micelle MC@ODA-CMD was prepared from distilled water without ethylenediamine as control.

4.1.4. Determination of encapsulation efficiency and drug-loading capacity

The freeze-dried drug-loaded micelles of 1 mg were dissolved in 3 mL DMSO under the condition without light exposure. The concentration was determined by ultraviolet spectrophotometer after dilution in a particular proportion. The encapsulation efficiency and drug-loading capacity were calculated by the following formula:

Drug-loading capacity (DL%) = (Amount of drug in micelles/Amount of micelles) × 100% (1)

Encapsulation efficiency (EE%) = (Amount of drug entrapped in micelles/Total amount of drug used for micelles preparation) × 100% (2)

Preprints (www.preprints.org) | NOT PEER-REVIEWED | Posted: 8 November 2021 doi:10.20944/preprints202111.0155.v1

4.1.5. Determination of particle size and Zeta potential of drug-loaded micelles

An adequate amount of drug-loaded micelle was dissolved in distilled water, and the micellar solution with a concentration of about 1 mg/mL was filtered by a 0.22 μm filter membrane. The particle size and Zeta potential were measured by Zeta potential and nanoparticle size analyzer, and the average value was obtained three times.

4.1.6. Determination of CMC of polymer materials

The value of CMC is an important index of micelle stability measured by the pyrene fluorescence probe method. 0.1 μmol/L pyrene stock solution was prepared with acetone, and 100 mg ODA-CMD was dissolved in 10 mL distilled water to obtain 10 mg/mL stock solution. The stock solution was then diluted to 10, 5, 1, 0.5, 0.1, 0.05, 0.01, 0.005, 0.001, 0.0005, 0.0001, 0.00005, 0.00001 mg/mL, and 50μL pyrene solution was added with incubation in a water bath at 37℃ for 6 h. After acetone is completely volatilized, the fluorescence intensities I394 and I373 were detected using a fluorescence spectrophotometer (Shanghai Precision and Scientific Instrument Co. Ltd, Shanghai, China) at an excitation wavelength of 339 nm and an emission wavelength of 373 nm and 394 nm. The curve was developed using concentration as vertical coordinate and the I394/I373 as horizontal coordinate, and the inflection point was taken as CMC. The CMC measurement of (ODA-CMD)$_{CL}$ is the same as above.

4.2. Evaluation of biocompatibility of micellar materials

4.2.1. Blank micelle hemolysis assay

8 mL of rabbit blood was added with a certain amount of heparin (Sigma-Aldrich, St Louis, USA) for anticoagulation and then diluted with 10 mL of normal saline. 100 μL diluted blood was added to different concentrations of 1 mL micellar solution, and after a warm bath at 37°C for a certain period, centrifuged at 750g for 5 min. The supernatant was added to 2 mL ethanol/hydrochloric acid mixture (39:1; 99% ethanol (v/v):37% hydrochloric acid (w/v), after centrifugation for another 5 min, the supernatant was taken. The absorbance was measured at 398 nm by an ultraviolet spectrophotometer (TU-1901, Beijing Puekinje Co., China). The positive control was distilled water, and the negative control was 0.9% normal saline, all of which were treated with the same method. The hemolysis rate of micelle solution (HR%) was calculated by the following formula:

$$HR\ (\%) = (A\ test - A\ negative)/(A\ positive - A\ negative) \times 100\% \quad (3)$$

In which, A test is the absorbance of the experiment tube. A negative is the absorbance of the negative control tube. A positive is the absorbance of the positive control tubes.

4.2.2. Blank micelle cytotoxicity assay

In this study, the safety of micellar materials was evaluated by detecting the toxic effect of micellar materials on human umbilical vein endothelial cells (HUVECs) (Institute of Biochemistry and Cell Biology, Chinese Academy of Science, Shanghai, China). HUVECs were suspended in RPMI-1640 (HyClone, UT, USA) medium containing 10% fetal bovine serum (HyClone, UT, USA) and incubated in 37 °C, 5% CO2 incubator. The logarithmic growth phase cells were inoculated in a 96-Well culture plate and cultured overnight in a CO2 incubator. The culture medium was absorbed, different concentrations of blank micelle solution were added and incubated for 24 h. Then 20 μL 3-(4,5-Dimethylthiazol-2-yl)-2,5-diphenyltetrazolium bromide (MTT) (J&K Scientific Ltd, Beijing, China) solution (5 mg/mL) was added and incubated for 4 h. The culture medium was discarded, and 200 μL DMSO was added. The absorbance at 490 nm was measured with a microplate reader (BioRad Laboratories, Inc. CA, USA). Survival Rates= (Absorbance value after administration/Absorbance value of negative control) × 100%. The survival curve was developed with drug concentration as the horizontal ordinate and survival rates as the vertical ordinate.

Preprints (www.preprints.org) | NOT PEER-REVIEWED | Posted: 8 November 2021 doi:10.20944/preprints202111.0155.v1

4.3. Fabrication and in vitro release test of titanium specimens

4.3.1. Smooth polished titanium

Commercially pure titanium sheet (Northwest Institute for Non-ferrous Metal Research, Xi'an, People's Republic of China) in disk form (10 mm in diameter and 2 mm in thickness） were mechanically ground by 400-7,000 grit silicon carbide paper and cleaned ultrasonically in acetone (FUYU Fine Chemicals Co., Ltd.), ethanol and deionized water.

4.3.2. MAO treatment

The MAO procedure was carried out in a mixed aqueous solution containing 0.04 M β-glycerophosphate sodium (Ruixi Biological Technology Co., Ltd., Xi'an, People's Republic of China) and 0.2 M calcium acetate (Ruixi Biological Technology Co., Ltd.) using a pulsed direct current power supply. The applied voltage, oxidizing time, frequency, duty cycle were 300V, 5 minutes, 600 Hz, 8.0%, respectively. The surface morphology of MAO titanium was observed by scanning electron microscope (SEM) after the specimens were rinsed with deionized water and air-dried.

4.3.3. MAO treatment

The drug-loaded micelles with 600ug MC were added to the 1mL of 0.2% gelatin solution, and the suspension was formed by ultrasonic treatment for 10 min. The suspension was dropwise added and evenly laid on the surface of the titanium sheet with a diameter of 1cm, shaken for 1 hour, and dried. The titanium surface was washed with ethanol three times and freeze-dried.

4.3.4. In vitro release test of drug-loaded micellar coating on titanium surface

In this study, the pH7.4 PBS was used as the release medium. Drug release experiment was carried out using the dialysis bag method. 2 mL containing an equal dose of free MC, MC-loaded nanomicelles (MC@ODA-CMD), MC-loaded crosslinked nanomicelles (MC@(ODA-CMD)$_{CL}$), MC-loaded MAO-Ti, MC@ODA-CMD loaded MAO-Ti, MC@(ODA-CMD)$_{CL}$ loaded MAO-Ti were loaded into dialysis bags (3500 g/mol), placed in an Eppendorf (EP) tube containing a 5mL release medium and shaken in a constant temperature oscillator (37 °C, 60rpm). Samples were taken at the preset time point (1h, 12h, 24h, 3d, 5d, 9d, 11d and 15d), and all the release media in the release tube were replaced with fresh media to ensure that the leakage condition of minocycline could be met. The drug content in the sample was determined by ultraviolet spectrophotometry, and the cumulative release percentage of the drug was calculated.

4.4. Antibacterial effect of drug-loaded micellar coating on titanium

4.4.1. Antibacterial rate (AR)

Staphylococcus aureus (S.aureus) (ATCC 25923; ATCC, Manassas, VA, USA) was cultured in Mueller-Hinton medium (Aobox Biotechnology, Beijing, People's Republic of China) until the mid-logarithmic period. The bacterial solution was adjusted to a concentration of 106 CFU/mL. The specimens (S-Ti, MAO-Ti and MC@ (ODA-CMD) CL-Ti) were incubated in 1mL of the bacterial suspension at 37 °C for 24 hours, respectively. Each titanium specimen was then rinsed twice with PBS. The bacteria attached to the specimens were isolated with 5mL of PBS solution for 5 minutes. The bacterial suspensions were recultivated on Mueller-Hinton agar (MHA) plates for colony counting. The AR was calculated as follows:

$$AR\ (\%) = (CFU_{control} - CFU_{experiment}) / CFU_{control} \times 100\% \quad (4)$$

In which S-Ti served as the control group, MAO-Ti and MC@ (ODA-CMD) CL-Ti constituted the experimental groups.

Preprints (www.preprints.org) | NOT PEER-REVIEWED | Posted: 8 November 2021 doi:10.20944/preprints202111.0155.v1

4.4.2. Bacterial viability

The specimens (S-Ti, MAO-Ti and MC@(ODA-CMD)$_{CL}$-Ti) were incubated in 1mL of bacterial suspension(106 CFU/mL) for 24 hours, then rinsed thrice with PBS and stained with SYTO ® 9 and propidium iodide dyed (LIVE/ DEAD BacLightTM Bacterial Viability Kits L13152; Life Technologies Corp, Carlsbad, CA, USA) for 15 minutes without light exposure. The live bacteria (intact membranes) were stained by SYTO 9 (green), and the dead bacteria (membranes damaged) were stained by propidium iodide (red), followed by examination using laser scanning confocal microscopy (FV1000; Olympus, Tokyo, Japan).

4.5. Statistical analysis

All of the experiments were repeated in parallel at least three times, and data were presented as mean ± standard deviation. Statistical analysis was performed using Prism 9.2.0 (GraphPad Software, La Jolla, CA, USA) with one-way or two-way analysis of variance (ANOVA). Statistical significance was considered at $P < 0.05$.

5. Conclusions

In this study, we developed an amphiphilic nanomicelles based on carboxymethyl ODA and CMD. After being loaded with MC and fabricated on the MAO-Ti surface, the antibacterial coating maintained long-term drug release ability and showed significant antibacterial activity against gram-positive *S.aureus.* Moreover, the nanomicelles were proved to be biocompatible and non-toxic. It can be suggested that the application of this antibacterial coating may be a potential strategy to prevent implant-related infection.

Author Contributions: Writing—original draft preparation, M.Z. and H.W.; writing—review and editing, H.W., W.Y. and M.Z.; funding acquisition, H.W.; investigation, M.Z., L.Z. and J.Y.; visualization, H.W., M.Z.,and W.Y.; supervision, H.W. and W.Y. All authors have read and agreed to the published version of the manuscript.

Funding: This research was funded by the National Natural Science Foundation of China (81901869) ,the Natural Science Foundation of Shaanxi Province (2019JM-374) .

Institutional Review Board Statement: Not applicable

Informed Consent Statement: Not applicable

Data Availability Statement: Data are available from correspondent authors.

Acknowledgments: Graphical abstract was created with BioRender.com

Conflicts of Interest: The authors declare no conflict of interest.

References

1. Dreyer, H.; Grischke, J.; Tiede, C.; Eberhard, J.; Schweitzer, A.; Toikkanen, S.E.; Glöckner, S.; Krause, G.; Stiesch, M. Epidemiology and risk factors of peri-implantitis: A systematic review. *J Periodontal Res* **2018**, *53*, 657-681, doi:10.1111/jre.12562.
2. Rakic, M.; Galindo-Moreno, P.; Monje, A.; Radovanovic, S.; Wang, H.-L.; Cochran, D.; Sculean, A.; Canullo, L. How frequent does peri-implantitis occur? A systematic review and meta-analysis. *Clin Oral Investig* **2018**, *22*, 1805-1816, doi:10.1007/s00784-017-2276-y.

Preprints (www.preprints.org) | NOT PEER-REVIEWED | Posted: 8 November 2021 doi:10.20944/preprints202111.0155.v1

3. Lee, C.-T.; Huang, Y.-W.; Zhu, L.; Weltman, R. Prevalences of peri-implantitis and peri-implant mucositis: systematic review and meta-analysis. *J Dent* **2017**, *62*, doi:10.1016/j.jdent.2017.04.011.
4. Chrcanovic, B.R.; Albrektsson, T.; Wennerberg, A. Periodontally compromised vs. periodontally healthy patients and dental implants: a systematic review and meta-analysis. *J Dent* **2014**, *42*, 1509-1527, doi:10.1016/j.jdent.2014.09.013.
5. Costerton, J.W.; Stewart, P.S.; Greenberg, E.P. Bacterial biofilms: a common cause of persistent infections. *Science* **1999**, *284*, 1318-1322.
6. Isackson, D.; McGill, L.D.; Bachus, K.N. Percutaneous implants with porous titanium dermal barriers: an in vivo evaluation of infection risk. *Med Eng Phys* **2011**, *33*, 418-426, doi:10.1016/j.medengphy.2010.11.007.
7. D'Haese, J.; Ackhurst, J.; Wismeijer, D.; De Bruyn, H.; Tahmaseb, A. Current state of the art of computer-guided implant surgery. *Periodontol 2000* **2017**, *73*, 121-133, doi:10.1111/prd.12175.
8. Izquierdo-Barba, I.; Vallet-Regí, M.; Kupferschmidt, N.; Terasaki, O.; Schmidtchen, A.; Malmsten, M. Incorporation of antimicrobial compounds in mesoporous silica film monolith. *Biomaterials* **2009**, *30*, 5729-5736, doi:10.1016/j.biomaterials.2009.07.003.
9. Holt, B.M.; Betz, D.H.; Ford, T.A.; Beck, J.P.; Bloebaum, R.D.; Jeyapalina, S. Pig dorsum model for examining impaired wound healing at the skin-implant interface of percutaneous devices. *J Mater Sci Mater Med* **2013**, *24*, 2181-2193, doi:10.1007/s10856-013-4975-5.
10. Cheng, Y.; Zhao, X.; Liu, X.; Sun, W.; Ren, H.; Gao, B.; Wu, J. Antibacterial activity and biological performance of a novel antibacterial coating containing a halogenated furanone compound loaded poly(L-lactic acid) nanoparticles on microarc-oxidized titanium. *Int J Nanomedicine* **2015**, *10*, 727-737, doi:10.2147/IJN.S75706.
11. Chouirfa, H.; Bouloussa, H.; Migonney, V.; Falentin-Daudré, C. Review of titanium surface modification techniques and coatings for antibacterial applications. *Acta Biomater* **2019**, *83*, 37-54, doi:10.1016/j.actbio.2018.10.036.
12. Allison, K.R.; Brynildsen, M.P.; Collins, J.J. Metabolite-enabled eradication of bacterial persisters by aminoglycosides. *Nature* **2011**, *473*, 216-220, doi:10.1038/nature10069.
13. Schilcher, K.; Horswill, A.R. Staphylococcal Biofilm Development: Structure, Regulation, and Treatment Strategies. *Microbiol Mol Biol Rev* **2020**, *84*, doi:10.1128/MMBR.00026-19.
14. Çalışkan, N.; Bayram, C.; Erdal, E.; Karahaliloğlu, Z.; Denkbaş, E.B. Titania nanotubes with adjustable dimensions for drug reservoir sites and enhanced cell adhesion. *Mater Sci Eng C Mater Biol Appl* **2014**, *35*, 100-105, doi:10.1016/j.msec.2013.10.033.
15. Wang, J.; Wu, G.; Liu, X.; Sun, G.; Li, D.; Wei, H. A decomposable silica-based antibacterial coating for percutaneous titanium implant. *Int J Nanomedicine* **2017**, *12*, 371-379, doi:10.2147/IJN.S123622.
16. Zhu, M.-L.; Xu, X.-L.; Wang, X.-J.; Zhang, N.-N.; Lu, K.-J.; Qi, J.; Jin, F.-Y.; Liu, D.; Du, Y.-Z. Sialic-Acid-Anchored Micelles: A Hierarchical Targeting Device for Enhanced Tumor Tissue Accumulation and Cellular Internalization. *Mol Pharm* **2018**, *15*, 4235-4246, doi:10.1021/acs.molpharmaceut.8b00649.
17. Yao, Q.; Liu, Y.; Kou, L.; Tu, Y.; Tang, X.; Zhu, L. Tumor-targeted drug delivery and sensitization by MMP2-responsive polymeric micelles. *Nanomedicine* **2019**, *19*, 71-80, doi:10.1016/j.nano.2019.03.012.
18. Xi, Y.; Jiang, T.; Yu, Y.; Yu, J.; Xue, M.; Xu, N.; Wen, J.; Wang, W.; He, H.; Shen, Y.; et al. Dual targeting curcumin loaded alendronate-hyaluronan- octadecanoic acid micelles for improving osteosarcoma therapy. *Int J Nanomedicine* **2019**, *14*, 6425-6437, doi:10.2147/IJN.S211981.
19. Mei, L.; Rao, J.; Liu, Y.; Li, M.; Zhang, Z.; He, Q. Effective treatment of the primary tumor and lymph node metastasis by polymeric micelles with variable particle sizes. *J Control Release* **2018**, *292*, 67-77, doi:10.1016/j.jconrel.2018.04.053.
20. Gote, V.; Mandal, A.; Alshamrani, M.; Pal, D. Self-Assembling Tacrolimus Nanomicelles for Retinal Drug Delivery. *Pharmaceutics* **2020**, *12*, doi:10.3390/pharmaceutics12111072.

Preprints (www.preprints.org) | NOT PEER-REVIEWED | Posted: 8 November 2021 doi:10.20944/preprints202111.0155.v1

21. Xu, H.; Yao, Q.; Cai, C.; Gou, J.; Zhang, Y.; Zhong, H.; Tang, X. Amphiphilic poly(amino acid) based micelles applied to drug delivery: The in vitro and in vivo challenges and the corresponding potential strategies. *Journal of Controlled Release* **2015**, *199*, 84-97, doi:https://doi.org/10.1016/j.jconrel.2014.12.012.
22. Anirudhan, T.S.; Binusreejayan. Dextran based nanosized carrier for the controlled and targeted delivery of curcumin to liver cancer cells. *International Journal of Biological Macromolecules* **2016**, *88*, 222-235, doi:https://doi.org/10.1016/j.ijbiomac.2016.03.040.
23. Wasiak, I.; Kulikowska, A.; Janczewska, M.; Michalak, M.; Cymerman, I.A.; Nagalski, A.; Kallinger, P.; Szymanski, W.W.; Ciach, T. Dextran Nanoparticle Synthesis and Properties. *PLoS One* **2016**, *11*, e0146237, doi:10.1371/journal.pone.0146237.
24. Cha, J.K.; Lee, J.S.; Kim, C.S. Surgical Therapy of Peri-Implantitis with Local Minocycline: A 6-Month Randomized Controlled Clinical Trial. *J Dent Res* **2019**, *98*, 288-295, doi:10.1177/0022034518818479.
25. Jepsen, S.; Berglundh, T.; Genco, R.; Aass, A.M.; Demirel, K.; Derks, J.; Figuero, E.; Giovannoli, J.L.; Goldstein, M.; Lambert, F.; et al. Primary prevention of peri-implantitis: managing peri-implant mucositis. *Journal of clinical periodontology* **2015**, *42 Suppl 16*, S152-S157, doi:10.1111/jcpe.12369.
26. Huang, Y.; Ding, X.; Qi, Y.; Yu, B.; Xu, F.-J. Reduction-responsive multifunctional hyperbranched polyaminoglycosides with excellent antibacterial activity, biocompatibility and gene transfection capability. *Biomaterials* **2016**, *106*, 134-143, doi:10.1016/j.biomaterials.2016.08.025.
27. Berglundh, T.; Lindhe, J.; Ericsson, I.; Marinello, C.P.; Liljenberg, B.; Thomsen, P. The soft tissue barrier at implants and teeth. *Clin Oral Implants Res* **1991**, *2*, 81-90.
28. Moon, I.S.; Berglundh, T.; Abrahamsson, I.; Linder, E.; Lindhe, J. The barrier between the keratinized mucosa and the dental implant. An experimental study in the dog. *Journal of clinical periodontology* **1999**, *26*, 658-663.
29. Wang, Y.; Zhang, Y.; Miron, R.J. Health, Maintenance, and Recovery of Soft Tissues around Implants. *Clin Implant Dent Relat Res* **2016**, *18*, 618-634, doi:10.1111/cid.12343.
30. Romanò, C.L.; Scarponi, S.; Gallazzi, E.; Romanò, D.; Drago, L. Antibacterial coating of implants in orthopaedics and trauma: a classification proposal in an evolving panorama. *J Orthop Surg Res* **2015**, *10*, 157, doi:10.1186/s13018-015-0294-5.
31. Katsumiti, A.; Gilliland, D.; Arostegui, I.; Cajaraville, M.P. Mechanisms of Toxicity of Ag Nanoparticles in Comparison to Bulk and Ionic Ag on Mussel Hemocytes and Gill Cells. *PLoS One* **2015**, *10*, e0129039, doi:10.1371/journal.pone.0129039.
32. Wei, H.; Wu, S.; Feng, Z.; Zhou, W.; Dong, Y.; Wu, G.; Bai, S.; Zhao, Y. Increased fibroblast functionality on CNN2-loaded titania nanotubes. *Int J Nanomedicine* **2012**, *7*, 1091-1100, doi:10.2147/ijn.S28694.
33. Gungor, S.; Kahraman, E.; Ozsoy, Y. Polymeric micelles for cutaneous drug delivery. IAPC Publishing: 2015; pp. 367-387.
34. Hu, Q.; Lu, Y.; Luo, Y. Recent advances in dextran-based drug delivery systems: From fabrication strategies to applications. *Carbohydrate polymers* **2021**, *264*, 117999, doi:10.1016/j.carbpol.2021.117999.
35. Shingel, K.I. Determination of structural peculiarities of dexran, pullulan and γ-irradiated pullulan by Fourier-transform IR spectroscopy. *Carbohydrate Research* **2002**, *337*, 1445-1451, doi:https://doi.org/10.1016/S0008-6215(02)00209-4.
36. Shingel, K.I. Current knowledge on biosynthesis, biological activity, and chemical modification of the exopolysaccharide, pullulan. *Carbohydrate Research* **2004**, *339*, 447-460, doi:https://doi.org/10.1016/j.carres.2003.10.034.
37. Arciola, C.R.; Campoccia, D.; Montanaro, L. Implant infections: adhesion, biofilm formation and immune evasion. *Nat Rev Microbiol* **2018**, *16*, 397-409, doi:10.1038/s41579-018-0019-y.
38. Foster, T.J.; Geoghegan, J.A.; Ganesh, V.K.; Höök, M. Adhesion, invasion and evasion: the many functions of the surface proteins of Staphylococcus aureus. *Nat Rev Microbiol* **2014**, *12*, 49-62, doi:10.1038/nrmicro3161.
39. van Winkelhoff, A.J. Antibiotics in the treatment of peri-implantitis. *Eur J Oral Implantol* **2012**, *5 Suppl*, S43-S50.

Preprints (www.preprints.org) | NOT PEER-REVIEWED | Posted: 8 November 2021 doi:10.20944/preprints202111.0155.v1

40. Qian, W.; Qiu, J.; Su, J.; Liu, X. Minocycline hydrochloride loaded on titanium by graphene oxide: an excellent antibacterial platform with the synergistic effect of contact-killing and release-killing. *Biomater Sci* **2018**, *6*, 304-313, doi:10.1039/c7bm00931c.
41. Shaki, H.; Ganji, F.; Kempen, P.J.; Dolatshahi-Pirouz, A.; Vasheghani-Farahani, E. Self-assembled amphiphilic-dextran nanomicelles for delivery of rapamycin. *Journal of Drug Delivery Science and Technology* **2018**, *44*, 333-341, doi:https://doi.org/10.1016/j.jddst.2018.01.010.
42. Nguyen, F.; Starosta, A.L.; Arenz, S.; Sohmen, D.; Dönhöfer, A.; Wilson, D.N. Tetracycline antibiotics and resistance mechanisms. *Biol Chem* **2014**, *395*, 559-575, doi:10.1515/hsz-2013-0292.
43. Renvert, S.; Lessem, J.; Dahlén, G.; Lindahl, C.; Svensson, M. Topical minocycline microspheres versus topical chlorhexidine gel as an adjunct to mechanical debridement of incipient peri-implant infections: a randomized clinical trial. *Journal of clinical periodontology* **2006**, *33*, 362-369.
44. Qian, W.; Qiu, J.; Liu, X. Minocycline hydrochloride-loaded graphene oxide films on implant abutments for peri-implantitis treatment in beagle dogs. *J Periodontol* **2020**, *91*, 792-799, doi:10.1002/JPER.19-0285.
45. Draye, J.-P.; Delaey, B.; Van de Voorde, A.; Van Den Bulcke, A.; De Reu, B.; Schacht, E. In vitro and in vivo biocompatibility of dextran dialdehyde cross-linked gelatin hydrogel films. *Biomaterials* **1998**, *19*, 1677-1687, doi:https://doi.org/10.1016/S0142-9612(98)00049-0.
46. Cadée, J.A.; van Luyn, M.J.; Brouwer, L.A.; Plantinga, J.A.; van Wachem, P.B.; de Groot, C.J.; den Otter, W.; Hennink, W.E. In vivo biocompatibility of dextran-based hydrogels. *J Biomed Mater Res* **2000**, *50*, 397-404.